ACS Sustainable Chemistry & Engineering

Research Article

pubs.acs.org/journal/ascecg

Facile Fabrication of Reduced Graphene Oxide/Polypyrrole Composite Hydrogels with Excellent Electrochemical Performance and Compression Capacity

Tao Ni, Liang Xu, Yupeng Sun, Wei Yao, Tingyang Dai,* and Yun Lu*

Department of Polymer Science and Engineering, State Key Laboratory of Coordination Chemistry, Key Laboratory of High Performance Polymer Materials and Technology of Ministry of Education, School of Chemistry and Chemical Engineering, Nanjing University, No. 22 Hankou Road, Gulou District, Nanjing, Jiangsu 210093, People's Republic of China

ABSTRACT: We report a facile method to fabricate reduced graphene oxide/polypyrrole hydrogels (rGO/PPy) simply by combining the self-assembly process at room temperature with oxidation polymerization at elevated temperature. The as-prepared composite hydrogels possess a cross-linked 3D hierarchical porous structure and show a compression-tolerant property and a high specific capacitance of 473 F g^{-1} at 1 A g^{-1}. In particular, 82% of the capacitance value has been maintained after charge−discharge for 5000 cycles, suggesting the great potential applications of the rGO/PPy hydrogels in high-quality energy storage devices. This study provides a novel reference way for the self-assembly of other conducting polymer and graphene sheets for different applications.

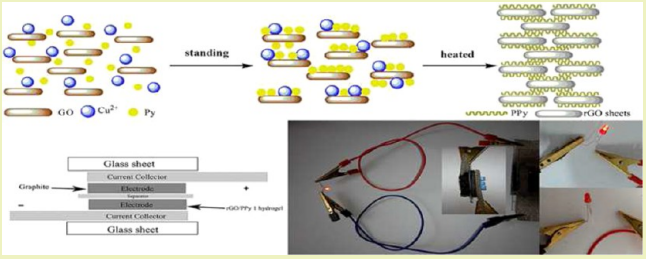

KEYWORDS: *Facile fabrication, Polypyrrole, Reduced graphene oxide, Composite hydrogels, Specific capacitance, Compression capacity*

INTRODUCTION

With the rapid development of the global economy, and thereby the continuous depletion of fossil fuels as well as increasing environmental pollution, to develop clean, efficient, sustainable sources of energy has become an important challenge. For electrochemical energy conversion and storage, supercapacitors have attracted considerable attention because of their high power density, long cycle life, low cost, and good environmental friendliness.[1] Graphene, a two-dimensional graphite sheet, is one of the most appropriate materials for supercapacitors due to its low mass density, excellent electrical properties, unusual mechanical strength, and high specific surface area.[2−5] Meanwhile, the novel structures of graphene materials have a significant impact upon the final electrochemical performance. For example, constructing a foam-like three-dimensional (3D) structure with high porosity, flexibility, and stablity under mechanical strain/stress has been verified as an effective approach for functional graphene materials.[6−21] However, the materials merely constituted by graphene are far away from meeting the demand of specific capacitor because carbon materials store charges mainly in an electrochemical double-layer formed at the interface between the electrode and the electrolyte, rather than in the bulk of the capacitive material. Thus, currently, there is a growing interest in the novel composites with a remarkable pseudocapacitance on the surface of carbon nanostructures.[22] Conducting polymers such as polypyrrole (PPy), polyaniline (PANI), poly(3,4-ethylenedioxythiophene) (PEDOT), and their derivatives, etc. are kinds of very important active materials for supercapacitors. They have high conductivity in doped state with advantages such as facile synthesis, low cost, good environmental stability, high storage capacity, and adjustable redox activity.[23−26] Unfortunately, the rapid degradation of conducting polymers may appear and become accelerated by possible overcharging/discharging during sustained operation. In this situation, introducing conducting polymers into the carbon materials could be a good strategy to achieve an optimal capacitive property. Although an inspiring performance of graphene/conducting polymer composites has been reported frequently in recent years,[27,28] we are still faced with how to simply construct the composites with 3D hierarchical porous structure.

Reduced graphene (rGO) has most of the excellent properties of graphene, thanks to its similar laminated structure with graphene, and also offers better dispersancy and binding force with other base materials due to the functional groups on its surface, which is conducive to construct various composites. The performance of rGO/conducting polymer composites will be greatly affected by the preparation condition and technology including oxidant kind and amount, ratio of reactants, reaction time, temperature, etc. And to continue to raise the quality level of this kind of composites by adjusting the optimized reaction condition and technology has also been our unswerving pursuit. On the basis of our previous research,[29] in this work, we develop the rGO/PPy composite hydrogel with an excellent electro-

Received: December 21, 2014
Revised: March 24, 2015
Published: April 3, 2015

DOI: 10.1021/sc500828t
ACS Sustainable Chem. Eng. 2015, 3, 862−870

chemical property and compression capacity by using a high concentration of pyrrole (Py) monomer and Cu^{2+} to provide a more solid gel structure and a technology with the first placement at room temperature and the subsequent reaction at elevated temperature to achieve the self-assembly and polymerization of Py, in turn, on rGO. In the forming process of composite hydrogels, Py monomers are used to reduce graphene oxide (GO) to rGO, while themselves are oxidized by Cu^{2+} to polymerize, providing the compression capacity. Meanwhile, rGO/PPy hydrogel is prepared conveniently in a gentle condition regardless of electrochemistry method, which is promising in large-scale production. As-prepared 3D assemblies show high specific capacitance (473 F g^{-1} at 1 A g^{-1}), fantastic cycling stability (82% after 5000 cycles) and excellent mechanical property (compression-tolerant), revealing that the rGO/PPy hydrogels may have great potential applications in high-performance energy storage devices.

EXPERIMENTAL SECTION

Materials. Analytically pure pyrrole was purchased from Aladdin Reagent and distilled before use. All other reagents were received as analytical grade and were used without further purification.

Preparation of Graphite Oxide (GO). GO was prepared by the modified Hummers method.[30] 3 g of active carbon (50 μm in diameter) was added to the solution containing 20 mL of concentrated H_2SO_4, 2.5 g of $K_2S_2O_8$, and 2.5 g of P_2O_5. The resulting mixture was heated to 80 °C and kept for 16 h, and then diluted with 200 mL of distilled water. The product was filtered, washed then with distilled water until the filtrate became neutral, and dried finally at room temperature to achieve constant weight. The as-prepared preoxidized graphite was put into 120 mL of concentrated H_2SO_4 with stirring, to which 15 g of $KMnO_4$ was added slowly to keep the system temperature below 20 °C. After the mixture was stirred at 35 °C for 16 h, the aforementioned system was diluted with 200 mL of distilled water, and then 0.5 L of distilled water and 10 mL of 30% H_2O_2 solution were added to the terminate the reaction. The obtained product GO was centrifuged and washed with 1 L of 1:10 HCl solution, and then subjected to dialysis for 1 week to completely remove metal ions and acids.

Preparation of rGO/PPy Composite Hydrogels. 30 mmol of Py was added into a 6 mL 10 mg/mL aqueous GO dispersion, which had been treated ultrasonically for 15 min to achieve the exfoliation of GO. Then, into this mixture was added different amounts (120, 60 mmol) of $CuCl_2$, and the mixture was stirred for 10 min to form a uniform blend. The above mixture was left for 24 h to form a hydrogel, which was further heated to 90 °C for 6 h to form the rGO/PPy hydrogels (noted as rGO/PPy 1, rGO/PPy 2 hydrogel with decreasing mass of $CuCl_2$). For comparison, two samples, namely the aqueous GO dispersion containing Py monomer with 120 mmol of $CuCl_2$ and without $CuCl_2$, respectively, were directly heated to 90 °C for 6 h to form the rGO/PPy hydrogels (noted as rGO/PPy 3 and rGO/PPy 4 in turn).

Characterization. The morphologies of the freeze-dried hydrogels were observed by scanning electron microscopy (SEM, Hitachi S-4800). Fourier transform infrared (FTIR) spectra were recorded on BrukerVECTOR22 spectrometer. The X-ray diffraction (XRD) patterns were acquired on a XRD-6000 instrument (Shimadzu, Japan) with Cu Kα radiation source. X-ray photoelectron spectroscopy (XPS) analysis was performed on a PHI 5000 Versaprobe system, using monochromatic Al Kα radiation (1486.6 eV) operating at 25 W. Electrochemical experiments were carried out on a CHI600 electrochemical workstation. The working electrode was prepared by casting a nafion-impregnated sample onto a carbon electrode with a diameter of 1 cm. Typically, 10 mg of composite was added to 20 mL of distilled water containing 1.9 mg of carbon black and 62 μL of nafion solution (0.01 wt % in water) and sonicated for 20 min, which was dropped then onto the carbon electrode and dried before the electrochemical test. The mass of the active substance was 0.2 mg. A three-electrode cell system was used to evaluate the electrochemical performance by cyclic voltammetry (CV), galvanostatic charge−discharge, and electrochemical impedance spectroscopy (EIS) techniques at room temperature. The electrolyte used is a 1 M HCl aqueous solution. A platinum sheet and a saturated calomel electrode (SCE) were used as the counter and the reference electrodes, respectively. Meanwhile, a two-electrode cell system was used to evaluate the electrochemical performance by cyclic voltammetry (CV) and galvanostatic charge−discharge. Two carbon electrodes were used in two-electrode system. The thickness of the composite electrodes is about 0.5 mm. When calculating the specific capacitance of the composite, only active component mass was taken into account. The electrical conductivity was measured via the four-probe method at room temperature (RTS-8 4-point robes resistivity measurement system, Probes Tech., China). The Brunauer−Emmett−Teller (BET) specific surface area and the pore size distribution for the freeze-dried hydrogels were measured with an ASAP 2020 analyzer (Micromeritics, USA) at 77 K.

RESULTS AND DISCUSSION

Figure 1 presents the FTIR spectra for GO, PPy, and rGO/PPy 1 hydrogel. For GO (Figure 1a), the peaks located at 1736, 1400,

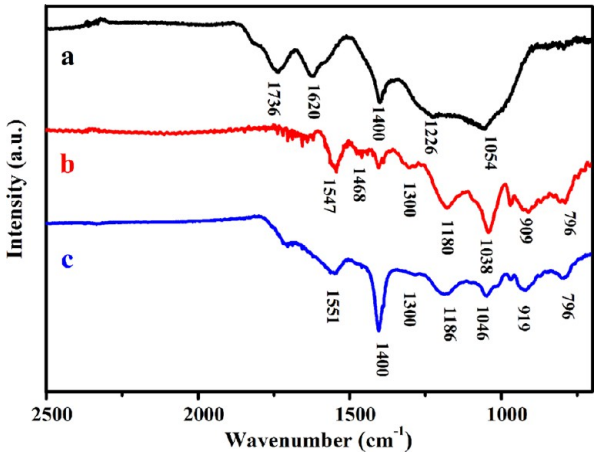

Figure 1. FTIR spectra of (a) GO, (b) PPy, and (c) rGO/PPy 1 hydrogel.

1226, and 1054 cm^{-1} pertain to the oxygen functional groups of GO such as −C═O/−COOH, C—OH, C—O—C, and C—O, respectively.[31] The vibration around 1620 cm^{-1} could be assigned to the adsorbed water molecules or descended from skeletal vibrations of unoxidized domain of GO.[32] For PPy (Figure 1b), the peaks situated at 1547 and 1468 cm^{-1} are ascribed to antisymmetric and symmetric ring-stretching modes, respectively. The peaks at 1300 and 1468 as well as 796 cm^{-1} are attributable to the C—H in-plane deformation vibration and C—H out-of-plane deformation vibration of the pyrrole ring in polymer, respectively. Also, the strong peaks around 1180 and 909 cm^{-1} represent the doping state of PPy.[33,34] Comparing to GO and PPy, the rGO/PPy 1 hydrogel shows the FTIR spectrum (Figure 1c) with the clear presence of the vibrational peaks assigned to PPy and the significant decrease in the intensity of adsorption bands belonging to the oxygen functional groups of GO, revealing the generation of PPy and the reduction of GO during the reaction process. It is noteworthy that, for rGO/PPy 1 hydrogel, some peaks assigned to PPy, such as antisymmetric ring-stretching, are up-shifted. The hydrogen bonding and $\pi-\pi$ interaction between the Py ring and rGO might be responsible for these spectral evolutions.

Figure 2 shows the XRD patterns of GO, PPy, and rGO/PPy 1 hydrogel. A diffraction peak appearing at around 2θ = 10.6° corresponding to an interplanar spacing of 8.31 Å[35] is clearly

DOI: 10.1021/sc500828t
ACS Sustainable Chem. Eng. 2015, 3, 862−870

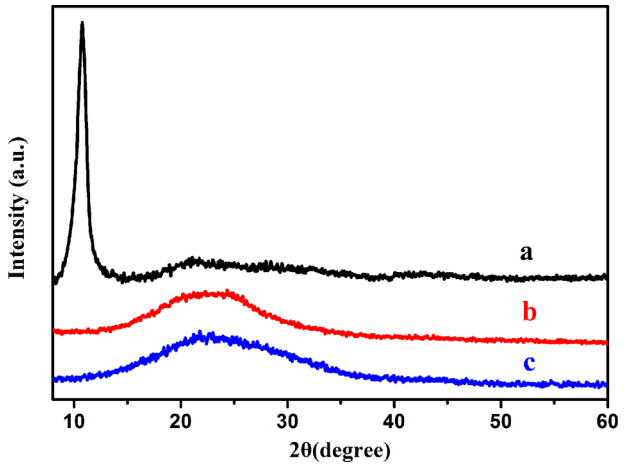

Figure 2. XRD patterns of (a) GO, (b)PPy, and (c) rGO/PPy 1 hydrogel.

shown in Figure 2a, which belongs to the [001] plane of GO.[36] Figure 2b exhibits a weak and broad diffraction peak in the region of $2\theta = 20-28°$, indicating the amorphous structural feature of PPy.[37] The similar broad diffraction peak only is also observed in Figure 2c confirming the existence of PPy and the vanishing of GO, which is consistent with the FTIR results. In the meantime, the broad diffraction peak also indicate that the rGO sheets is not closely packed.

GO and rGO/PPy 1 are also characterized by XPS spectra to evaluate intuitively the composition. Figure 3 presents XPS peaks attributed to C 1s for GO (Figure 3a) and rGO/PPy 1(Figure 3b), and to N 1s for rGO/PPy 1 (Figure 3c), respectively. By comparison, it is clear that after reaction the C—O/C═O unit almost disappears while part of N element is doped in rGO. The amounts of C, N, O, and Cu are summarized in Table 1 (72.7% rGO, 27.3% PPy). Just to be clear, only trace Cu element exists in rGO/PPy 1 hydrogels after dialysis, for Cu element has no contribution to electrochemical capacitor, the influence of Cu^{2+} could be ignored.

As we know, the volume of the rGO hydrogel generated from GO aqueous dispersion always less than that of the original GO dispersion system on account of the $\pi-\pi$ effect.[38] Interestingly, in our case, the obtained rGO/PPy composite hydrogel displays no volume contraction, which should relate with the microstructure of composite hydrogel. Figure 4a shows the SEM image of the GO with a paper-like structure, compared with which, the rGO prepared by normal thermal treatment method in the absence of Py displays a accumulate stratified structure (Figure

Table 1. Relative Amount (%) of Element in the GO and rGO/PPy 1 Hydrogels

sample	C	N	O	Cu
GO	69.2		30.8	
rGO/PPy 1	74.8	13.1	11.6	0.5

4b). By contrast, the rGO/PPy 1 hydrogel shows a well-defined and cross-linked 3D hierarchical porous structure (Figure 4c). The measured specific surface area of the composite hydrogel from the BET test is about 17 m^2/g, and the pore sizes are in the range of tens of nanometers to several micrometers, with an average pore size of 22 nm, which is obtained based on the Barrett—Joyner—Halenda (BJH) model. Such a mesoporous structure offers greater effective surface areas and facilitates the transport of electrons and ions.[39] It can also be seen that, from Figure 4c, in the hierarchical porous structure no PPy particles appear, although the concentration of Py and Cu^{2+} in the reaction system is very high. This feature is due to interactions between GO and Py, as well as the coordination between GO and Cu^{2+}, which makes the reaction take place only on the surface of GO. It is worth noting that GO may aggregate, causing precipitation under the condition of high concentration of salt solution.[30] So, the amount of salt added into GO aqueous dispersion is usually less, only equivalent to about 10% of that used in our case. Nevertheless, thanks to the interactions of GO sheets, bivalent copper ions and Py molecules, the obtained rGO disperse system displays its good stability even in the presence of high concentration Cu^{2+}. Moreover, the interactions limit the tropism of rGO sheets, weakening the $\pi-\pi$ effect and resulting the roseleaf shape microstructure. In view of this, the macroscopic volume of the formed composite hydrogel keeps consistent with that of initial reaction system after reacting. The FTIR spectra of GO (a) and the mixtures of GO/Cu^{2+} (b) and of GO/Py (c) shown in Figure 4d, in which the bands of COO^- and C—O vibration modes disappear, confirm the interaction between GO and Cu^{2+} as well as GO and Py supporting above discussions.

Based on the experimental results, it could be concluded that when the reaction system is placed for 16 h at room temperature the self-assembly of GO/Py and GO/Cu^{2+} is accomplished, even at the very slow rate of oxidation reaction of Py by Cu^{2+}, thus little PPy particles would form between GO sheets. When the reaction system is heated to 90 °C, the reaction of Py/Cu^{2+} speeds up, forming the hydrogels with cross-linked 3D hierarchical porous structure. The whole process is illustrated schematically in Figure 5.

CV, galvanostatic charge—discharge, and EIS techniques are used to test the electrochemical properties of the rGO/PPy 1

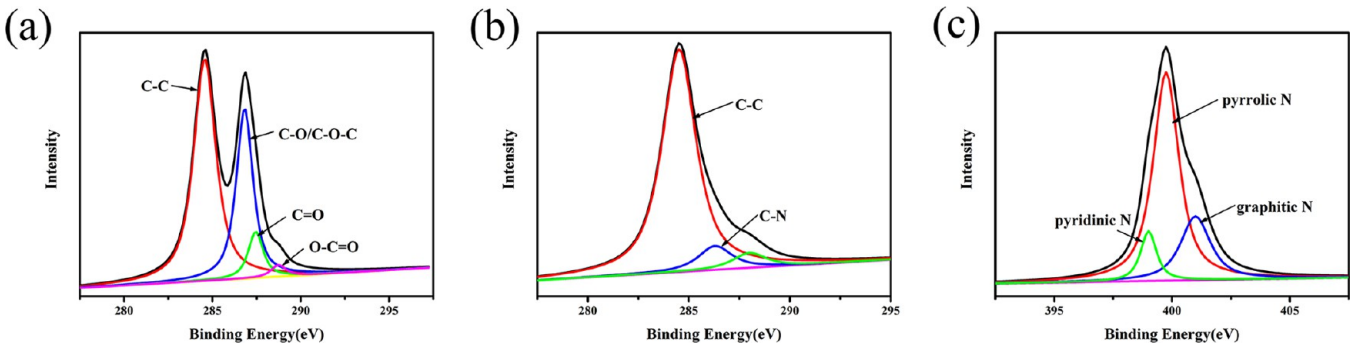

Figure 3. XPS spectra of (a) C 1s of GO, (b) C 1s, and (c) N 1s of rGO/PPy 1.

DOI: 10.1021/sc500828t
ACS Sustainable Chem. Eng. 2015, 3, 862—870

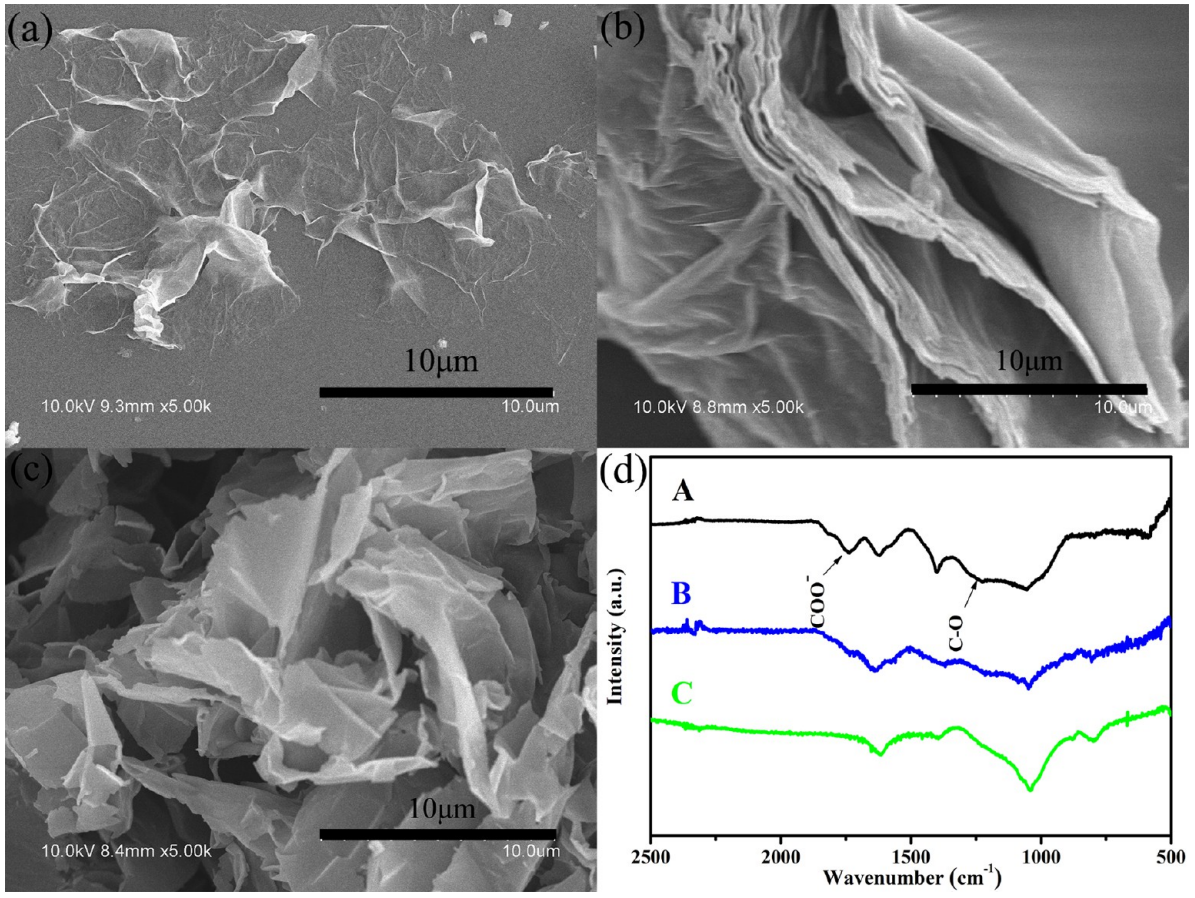

Figure 4. SEM images of (a) GO, (b) pure rGO prepared by thermal treatment in the absence of Py, and (c) rGO/PPy 1 hydrogel; (d) FTIR spectra of (A) GO, (B) GO/Py compound, and (C) GO/Cu^{2+} compound.

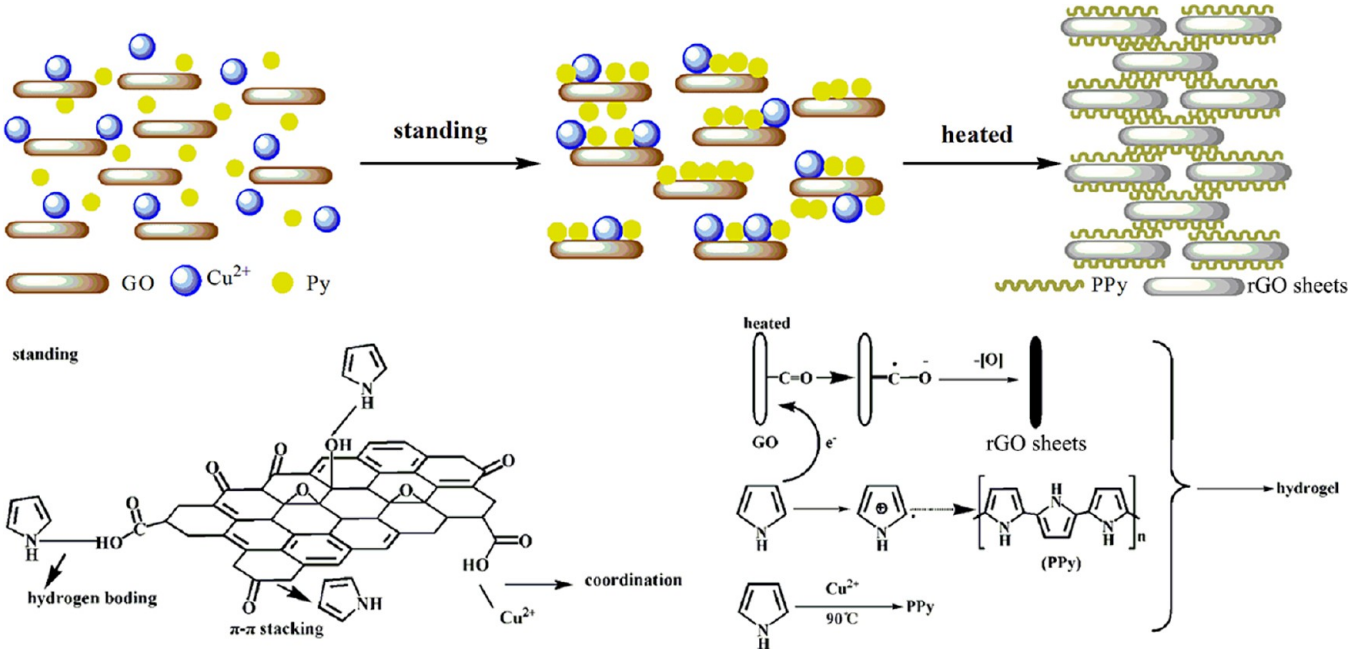

Figure 5. Schematic diagram of the preparation process of rGO/PPy 1 hydrogel.

hydrogel in three-electrode system. Figure 6a exhibits the CV spectra of the electrodes with a potential between 0 and 0.8 V (vs SCE). A nearly ideal rectangular shape at increasing voltage scanning rate from 5 to 100 mV s^{-1} is observed, showing almost perfect capacitive behavior. Investigating the electrochemical performance of the samples at high current density is used to evaluate whether the electrode materials are appropriate to any operation condition. Figure 6b shows the galvanostatic charge−

DOI: 10.1021/sc500828t
ACS Sustainable Chem. Eng. 2015, 3, 862−870

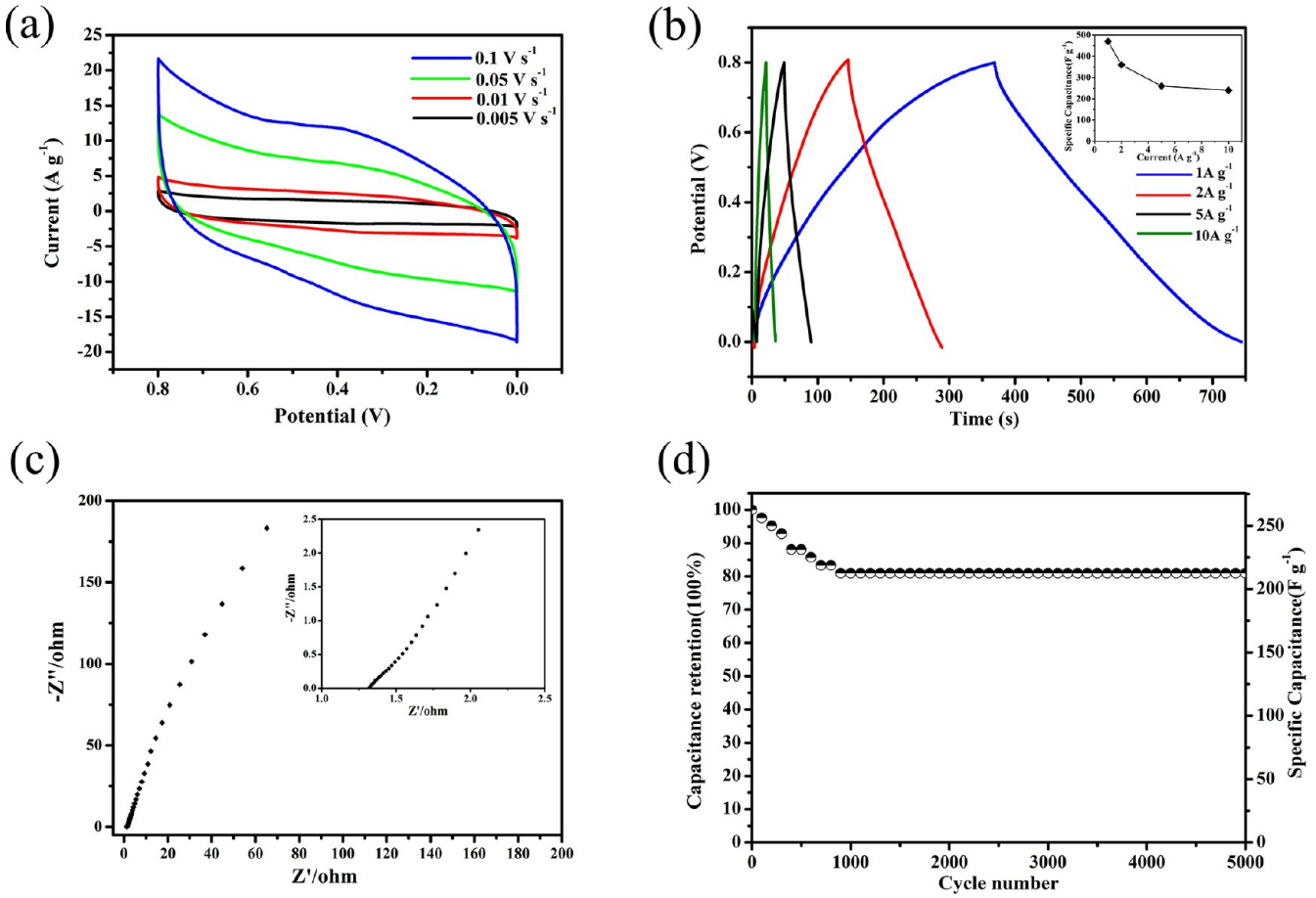

Figure 6. Electrochemical properties of the composite hydrogels (a) CV curves, (b) galvanostatic charge−discharge curves, specific capacitance at different current density (inset), (c) Nyquist impedance plots, and (d) cycle stability at a current density of 5 A g^{-1}.

discharge curves of the rGO/PPy 1 hydrogel at current densities from 1 to 10 A g^{-1} and the inset in Figure 6b shows the change in capacitance with current density. It can be seen that CV and the charge−discharge profile change with increasing scan and current rate. It might be owing to the restriction of the rate diffusion of electric charge. In fact, the Py monomer could not reduce GO totally to graphene due to its relative small reducing capacity, and thus may influence the conductivity of the composite (0.5 S·cm^{-1} in our case) and the electric charge transfer rate.[40] The rate performance of the composite hydrogels may also relate to the instability of PPy chains under large current. However, the specific capacitance of the composite hydrogel at the current of 10 A/g is larger than many rGO/conducting polymer composites reported.[13,28,29] The capacitance of rGO/PPy 1 hydrogel reaches 473 F g^{-1} at 1 A g^{-1}, making the rGO/PPy 1 hydrogel have a broad prospects in electrochemical capacitor.

Further electrochemical investigation is carried out to understand in depth the electrochemical performance of the rGO/PPy 1 hydrogel. The impedance spectrum of the rGO/PPy 1 hydrogel is shown as a Nyquist plot in Figure 6c. It is well-known that the Nyquist plots presents semicircles in low frequency with the diameters representing the charge-transfer resistance.[37,41] In the high frequency region, straight lines with the intercept at the *X*-axis represent the equivalent series resistance (ESR), which is related with the sum of the electrolyte solution resistance, the intrinsic resistance of active material, and the contact resistance at the electrode−electrolyte interface.[42] In our case, the ESR value is about 1 Ω (see the inset of Figure 6c), suggesting the high conductivity and enhanced capacitance properties of the hydrogels. The semicircle at the high frequency is so small that it could not be obviously seen, implying that the interfacial charge-transfer resistance is significantly low. A vertical plot at lower frequencies indicates a pure capacitive behavior with the fast ion diffusion in the electrode structure.[43] Figure 6d reveals the cycle life for rGO/PPy 1 hydrogel at the constant charge−discharge current density of 5 A g^{-1}. It is seen that the specific capacitance decreases only 18% after 1000 cycles, and maintains at a very stable value until 5000 cycles. Compared with pure conducting polymer materials which show a decrease in the specific capacitance more than 70% after only 2000 cycles,[44] the cycle stability of rGO/PPy 1 hydrogel in the long-term charge−discharge process is much improved. This is attributed to the rGO component with the superior chemical and electrochemical stability and the high mechanical strength, acting as an elastic skeleton to prevent PPy chains from damage due to volume change of PPy chains. On the other hand, a little decrease in the initial stage may be imputed to the degradation of PPy chains in the composite hydrogels due to their swelling and shrinking in the charge−discharge process. In addition, the trace Cu^{2+} may also affect the specific capacitance of the composite, since PPy skeleton may shrink-swell with the intercalation and deintercalation of Cu^{2+} during the charge−discharge process.

CV and galvanostatic charge−discharge in a two-electrode system were used to show the electrochemical properties of the rGO/PPy 1 hydrogel in practical use. Figure 7a exhibits the CV

DOI: 10.1021/sc500828t
ACS Sustainable Chem. Eng. 2015, 3, 862−870

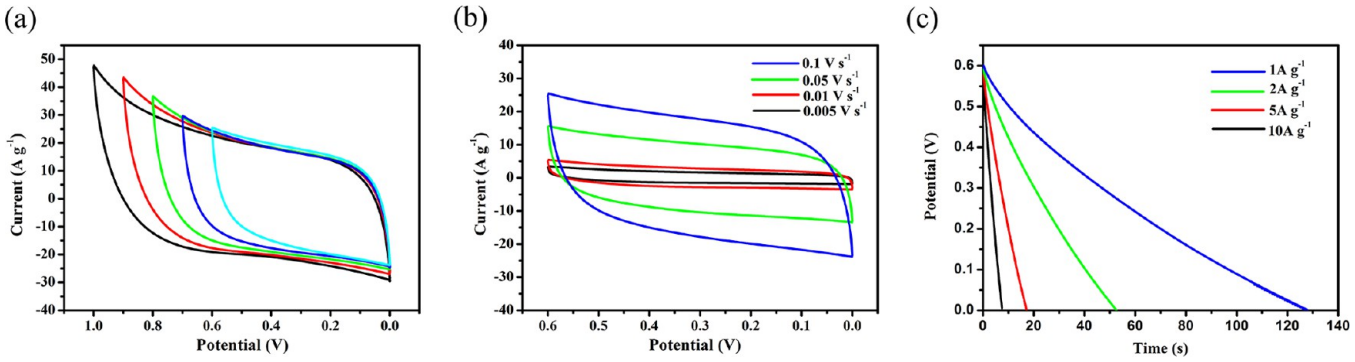

Figure 7. Electrochemical properties of the rGO/PPy 1 composite hydrogels in two-electrode system (a) CV curves from 0.6 to 1.0 V, (b) CV curves between 0 and 0.6 V, and (c) galvanostatic discharge curves.

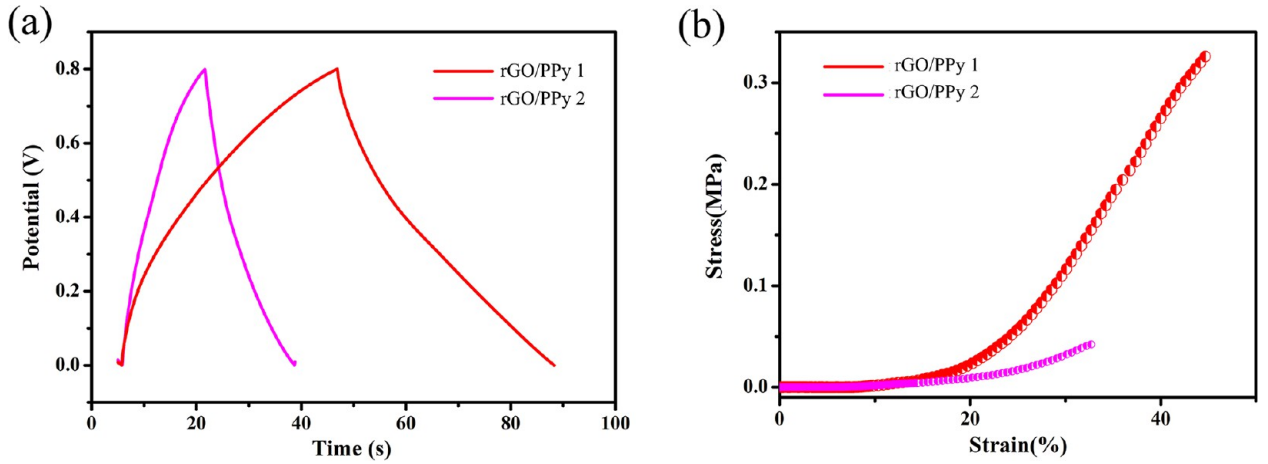

Figure 8. Comparison of rGO/PPy 1 and rGO/PPy 2 in electrochemical (galvanostatic charge−discharge curves at 5 A g^{-1}) and mechanical performance (compression strain).

curves from 0.6 to 1.0 V. When voltage is over 0.6 V, the overpotential phenomenon is more and more obvious with the increasing of voltage, indicating that the appropriate voltage should be less than 0.6 V. In addition, the shape of the CV curves also relate to the contribution of pseudocapacitance due to the existence of conducting PPy in the composite hydrogel. Figure 7b shows the CV curves of the electrodes with a potential between 0 and 0.6 V. The nearly ideal rectangular shape at increasing voltage scanning rate from 5 to 100 mV s^{-1} suggests that the rGO/PPy 1 hydrogel possesses perfect capacitive property. Based on the galvanostatic discharge curves of the rGO/PPy 1 hydrogel at current densities from 1 to 10 A g^{-1} (Figure 7c), the capacitance of rGO/PPy 1 hydrogel could be calculated according to the formula of $C = 4 \times (I \times \Delta t)/(M \times \Delta V)$, and reaches 433 F g^{-1} at 1 A g^{-1} and 250 F g^{-1} at 10 A g^{-1}, indicating its strong competitiveness in practical use as electrode materials.

rGO/PPy 1 and rGO/PPy 2 with different amounts of PPy were prepared to analyze the effect of PPy. Figure 8a is galvanostatic charge−discharge curves of rGO/PPy hydrogels at 5 A g^{-1}, which shows that the capacitance of rGO/PPy 1 is 2 times as much as that of rGO/PPy 2. The mechanical property of the hydrogels can be assessed by measuring the compressive stress−strain curves (Figure 8b). The J-shaped stress−strain curve of rGO/PPy 1 hydrogel displays an increase in compressive stress at the high strain region, and is postulated to be a signature of the improved mechanical strength.[45] The fracture stress reaches to 0.35 MPa, much higher than that of rGO/PPy 2. As we know, most of rGO/conducting polymer composite hydrogels have poor mechanical strength performance.[29,46] It is related to the morphology of the conducting polymers in the composites. In general, the PPy prepared by normal method easily form particles. Nevertheless, the PPy obtained in this work is a composite in which PPy chains combine with rGO, forming sheets rather than particles, and act as a bridge connecting the composite sheets to express a great mechanical strength performance. It could be thought that the more amount of PPy may lead to much denser structure and stronger interaction between PPy chains and rGO, resulting in the stronger mechanical property and the higher electrochemical performance at large current.

rGO/PPy 3 and rGO/PPy 4 were prepared to demonstrate the indispensability of the self-assembly of GO/Py and GO/Cu^{2+} at room temperature for formation of the rGO/PPy 1hydrogel. The CV (Figure 9a) and charge−discharge curves (Figure 9b) clearly exhibit that the electrochemical property of rGO/PPy 1 is much improved than that of rGO/PPy 3 and rGO/PPy 4. In the case of mechanical properties, the rGO/PPy 4 seems lost its all mechanical strength due to absence of Cu^{2+} to form adequate PPy for connecting GO sheets. The rGO/PPy 3 is similar to rGO/PPy 1 in appearance, but with the much lower mechanical strength and nearly zero compression-tolerant (Figure 9c). By contrast, the image (Figure 9d) shows the highly compression-rebound performance for rGO/PPy 1. As mentioned above, the amount of oxygen functional groups of GO was not enough for the oxidation of Py monomers in the formation of composite

DOI: 10.1021/sc500828t
ACS Sustainable Chem. Eng. 2015, 3, 862−870

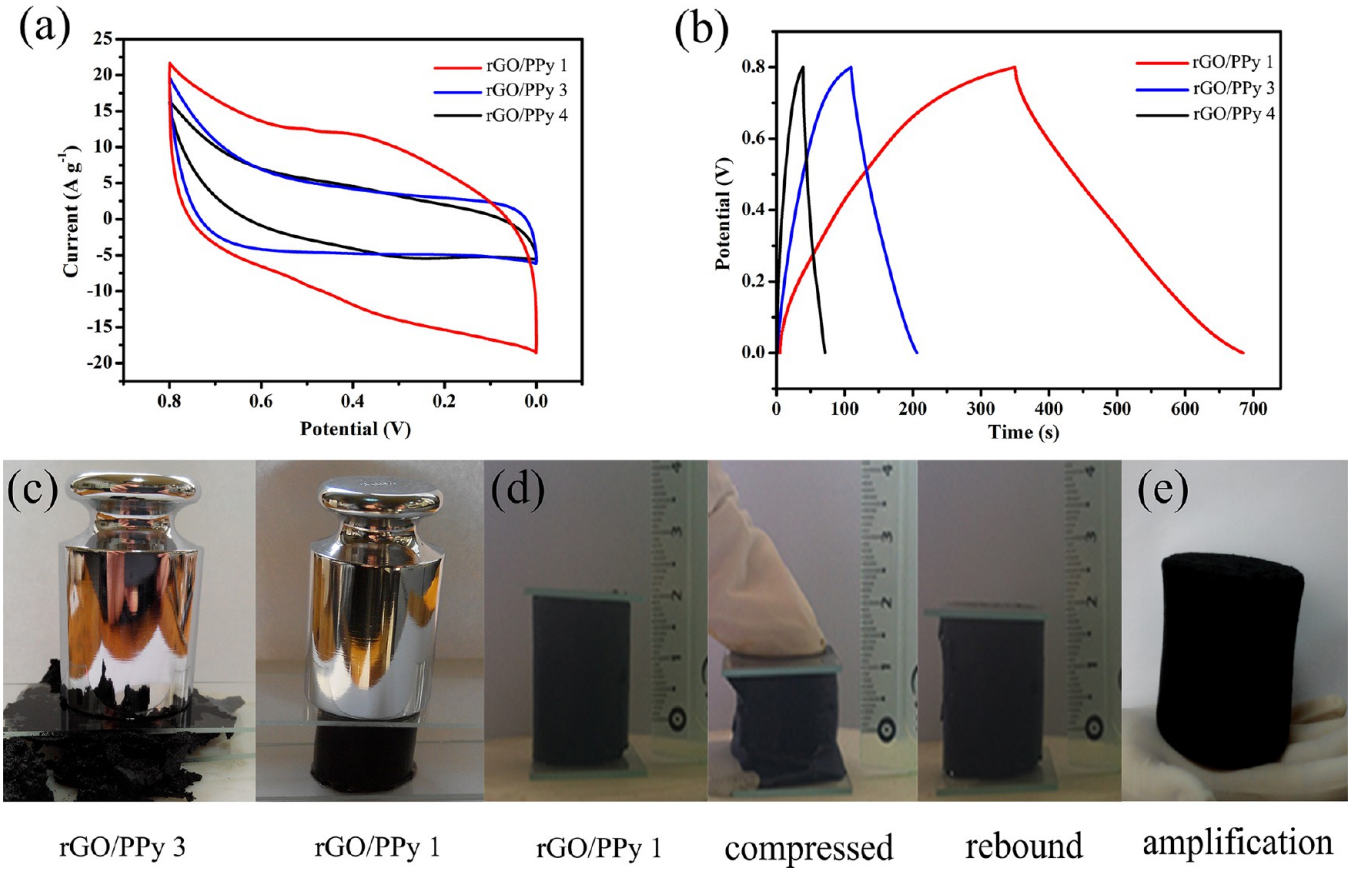

Figure 9. (a–b) Comparison of rGO/PPy 1, rGO/PPy 3, and rGO/PPy 4 in electrochemical performance; (c–d) comparison of rGO/PPy 1 and rGO/PPy 3 in compression performance; (e) rGO/PPy 1 with a size of 500 cm^3 obtained from the amplification reaction.

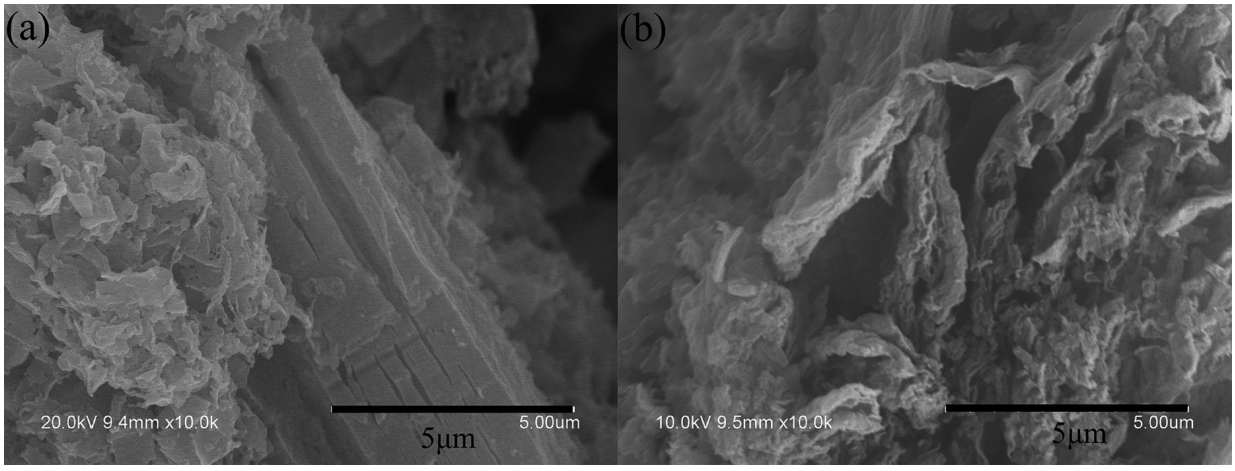

Figure 10. SEM images of rGO/PPy 3 (a) and rGO/PPy 4 (b).

hydrogels, so the additional oxidant such as Cu^{2+} is necessary. Also, the placing procedure for 16 h at room temperature is the key point for preparing rGO/PPy hydrogels with both high electrochemical and mechanical properties. This is because the reaction of Cu^{2+}/Py is competitive with that of GO/Py, thus hindering accomplishment of the self-assembly process, resulting in interior inhomogeneity just like rGO/PPy 3. The amplification reaction is succeeded, indicating that the rGO/PPy 1 hydrogel preparation process in the present work is appropriate for mass production (Figure 9e).

The differences of rGO/PPy 3 and rGO/PPy 4 hydrogels in structure and morphology are shown in Figure 10. It can be seen that from Figure 10a, rGO/PPy 3 displays obvious segregation phenomenon between the components in microstructure because PPy is oxidative polymerized directly by Cu^{2+} without accomplishing the self-assembly of Py on GO. It is the heterogeneity of microstructure that brings about the poor property of rGO/PPy 3, which proves again the necessity of placing process in the formation of rGO/PPy composite hydrogel. Figure 10b exhibits the microstructure of the rGO/PPy 4 hydrogel. In this case, on account of lacking enough

DOI: 10.1021/sc500828t
ACS Sustainable Chem. Eng. 2015, 3, 862–870

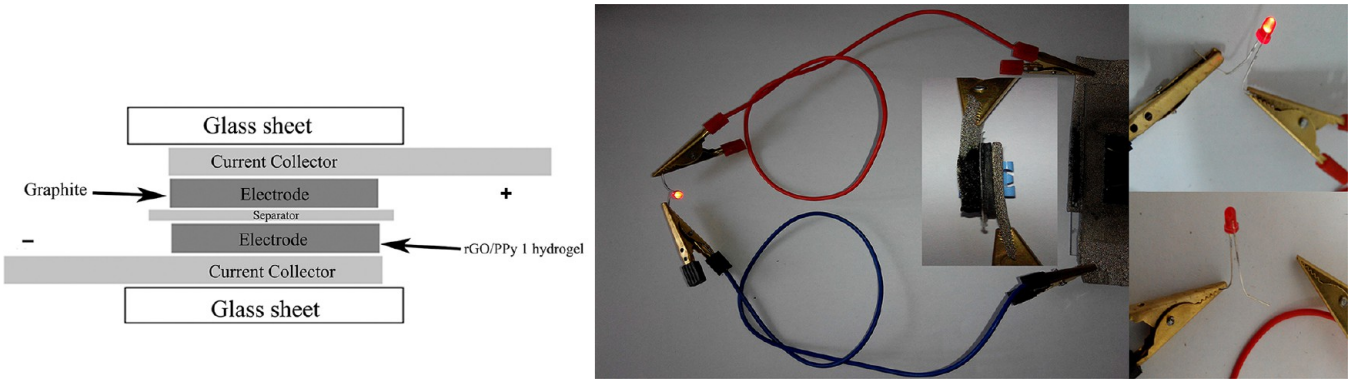

Figure 11. Analog device of a supercapacitor that successfully lights a LED.

oxidizing agent, there is not enough PPy to modify the rGO, which results in the accumulation of rGO. Meanwhile, insufficient PPy is difficult to play the role of bridging different rGO sheets, which leads to both poor mechanical and electrochemical properties.

An analog device of a supercapacitor was fabricated with the rGO/PPy 1 hydrogel as a negative electrode and graphite as a positive electrode. Successfully lighting a LED, as shown in Figure 11, reveals a great prospect of the composite hydrogels in practical use.

CONCLUSIONS

Composite hydrogels of rGO and PPy have been successfully prepared by a novel and facile method, in which the placing for hours for the reaction system at room temperature is an key process for the self-assembly of GO and Py to finally form the hydrogels with cross-linked 3D hierarchical porous structure. Also, the choice of $CuCl_2$ as an oxidant is also a key point for the reaction because the oxidation reaction of Py in the presence of Cu^{2+} can be easily controlled by changing the temperature. The as-prepared composite hydrogels could be the ideal candidate of electrode materials for supercapacitors due to their high specific capacitance, fantastic cycling stability, compression-tolerate property, and suitability for mass production. This study can be extended to the self-assembly of other conducting polymer and graphene sheets through simple route for different applications.

AUTHOR INFORMATION

Corresponding Authors

*Yun Lu. E-mail: yunlu@nju.edu.cn.

*Tingyang Dai. E-mail: daitingyang@163.com.

Notes

The authors declare no competing financial interest.

ACKNOWLEDGMENTS

This work was supported by the National Natural Science Foundation of China (Nos. 21174059, 21374046), China Postdoctoral Science Foundation (2013M530249), Program for Changjiang Scholars and Innovative Research Team in University, Open Project of State Key Laboratory of Supramolecular Structure and Materials (SKLSSM201416), and the Testing Foundation of Nanjing University.

REFERENCES

(1) Wang, G.; Zhang, L.; Zhang, J. A review of electrode materials for electrochemical supercapacitors. *Chem. Soc. Rev.* **2012**, *41* (2), 797–828.

(2) Allen, M. J.; Tung, V. C.; Kaner, R. B. Honeycomb carbon: A review of graphene. *Chem. Rev.* **2010**, *110*, 132–145.

(3) Eda, G.; Chhowalla, M. Chemically derived graphene oxide: Towards large-area thin-film electronics and optoelectronics. *Adv. Mater.* **2010**, *22* (22), 2392–2415.

(4) Geim, A. K.; Novoselov, K. S. The rise of graphene. *Nat. Mater.* **2007**, *6*, 183–191.

(5) Zhu, Y.; Murali, S.; Cai, W.; Li, X.; Suk, J. W.; Potts, J. R.; Ruoff, R. S. Graphene and graphene oxide: Synthesis, properties, and applications. *Adv. Mater.* **2010**, *22* (35), 3906–3924.

(6) Aliev, A. E.; Oh, J. Y.; Kozlov, M. E.; Kuznetsov, A. A.; Fang, S. L.; Fonseca, A. F.; Ovalle, R.; Lima, M. D.; Haque, M. D.; Gartstein, Y. N.; Zhang, M.; Zakhidov, A. A.; Baughman, R. H. Giant-stroke, superelastic carbon nanotube aerogel muscles. *Science* **2009**, *323* (20), 1575–1578.

(7) Anderson, M. L.; Stroud, R. M.; Rolison, R. D. Enhancing the activity of fuel-cell reactions by designing three-dimensional nanostructured architectures: Catalyst-modified carbon-silica composite aerogels. *Nano Lett.* **2002**, *2* (3), 235–240.

(8) Chen, Z.; Ren, W.; Gao, L.; Liu, B.; Pei, S.; Cheng, H. M. Three-dimensional flexible and conductive interconnected graphene networks grown by chemical vapour deposition. *Nat. Mater.* **2011**, *10* (6), 424–428.

(9) Cheng, C.; Li, D. Solvated graphenes: An emerging class of functional soft materials. *Adv. Mater.* **2013**, *25* (1), 13–30.

(10) Fan, Z.; Yan, J.; Zhi, L.; Zhang, Q.; Wei, T.; Feng, J.; Zhang, M.; Qian, W.; Wei, F. A three-dimensional carbon nanotube/graphene sandwich and its application as electrode in supercapacitors. *Adv. Mater.* **2010**, *22* (33), 3723–3728.

(11) Gui, X.; Wei, J.; Wang, K.; Cao, A.; Zhu, H.; Jia, Y.; Shu, Q.; Wu, D. Carbon nanotube sponges. *Adv. Mater.* **2010**, *22* (5), 617–621.

(12) Lee, C. K.; Shin, S. R.; Mun, J. Y.; Han, S. S.; So, I.; Jeon, J. H.; Kang, T. M.; Kim, S. I.; Whitten, P. G.; Wallace, G. G.; Spinks, G. M.; Kim, S. J. Tough supersoft sponge fibers with tunable stiffness from a DNA self-assembly technique. *Angew. Chem.* **2009**, *48* (28), 5116–5120.

(13) Li, C.; Shi, G. Functional gels based on chemically modified graphenes. *Advanced materials* **2014**, *26* (24), 3992–4012.

(14) Nardecchia, S.; Carriazo, D.; Ferrer, M. L.; Gutierrez, M. C.; del Monte, F. Three dimensional macroporous architectures and aerogels built of carbon nanotubes and/or graphene: Synthesis and applications. *Chem. Soc. Rev.* **2013**, *42* (2), 794–830.

(15) Niu, Z.; Chen, J.; Hng, H. H.; Ma, J.; Chen, X. A leavening strategy to prepare reduced graphene oxide foams. *Adv. Mater.* **2012**, *24* (30), 4144–4150.

(16) Svagan, A. J.; Samir, M. A. S. A.; Berglund, L. A. Biomimetic foams of high mechanical performance based on nanostructured cell walls reinforced by native cellulose nanofibrils. *Adv. Mater.* **2008**, *20* (7), 1263–1269.

(17) Vickery, J. L.; Patil, A. J.; Mann, S. Fabrication of graphene-polymer nanocomposites with higher-order three-dimensional architectures. *Adv. Mater.* **2009**, *21* (21), 2180–2184.

DOI: 10.1021/sc500828t
ACS Sustainable Chem. Eng. 2015, 3, 862–870

(18) Worsley, A. M.; Pauzauskie, P. J.; Olson, T. Y.; Biener, J.; Satcher, J. H.; Baumann, T. F. Synthesis of graphene aerogel with high electrical conductivity. *J. Am. Chem. Soc.* **2010**, *132*, 14067−14069.
(19) Xu, Y.; Wu, Q.; Sun, Y. Q.; Bai, H.; Shi, G. Q. Three-Dimensional Self-Assembly of Graphene Oxide and DNA into Multifunctional Hydrogels. *ACS Nano* **2010**, *4* (12), 7358−7362.
(20) Yang, X.; Qiu, L.; Cheng, C.; Wu, Y.; Ma, Z. F.; Li, D. Ordered gelation of chemically converted graphene for next-generation electroconductive hydrogel films. *Angew. Chem.* **2011**, *50* (32), 7325−7328.
(21) Zhang, L.; Shi, G. Preparation of highly conductive graphene hydrogels for fabricating supercapacitors with high rate capability. *J. Phys. Chem. C* **2011**, *115* (34), 17206−17212.
(22) Chabot, V.; Higgins, D.; Yu, A.; Xiao, X.; Chen, Z.; Zhang, J. A review of graphene and graphene oxide sponge: Material synthesis and applications to energy and the environment. *Energy Environ. Sci.* **2014**, *7* (5), 1564−1596.
(23) Kim, J.-H.; Sharma, A. K.; Lee, Y.-S. Synthesis of polypyrrole and carbon nano-fiber composite for the electrode of electrochemical capacitors. *Mater. Lett.* **2006**, *60* (13−14), 1697−1701.
(24) Liu, A.; Li, C.; Bai, H.; Shi, G. Q. Electrochemical deposition of polypyrrole/sulfonated graphene composite films. *J. Phys. Chem. C* **2010**, *114*, 22783−22789.
(25) Sharma, R. K.; Rastogi, A. C.; Desu, S. B. Manganese oxide embedded polypyrrole nanocomposites for electrochemical supercapacitor. *Electrochim. Acta* **2008**, *53* (26), 7690−7695.
(26) Vernitskaya, T. V.; Efimov, O. N. Polypyrrole: A conducting polymer; its synthesis, properties and applications. *Russ. Chem. Rev.* **1997**, *66* (5), 443−457.
(27) Zhao, Y.; Liu, J.; Hu, Y.; Cheng, H.; Hu, C.; Jiang, C.; Jiang, L.; Cao, A.; Qu, L. Highly compression-tolerant supercapacitor based on polypyrrole-mediated graphene foam electrodes. *Adv. Mater.* **2013**, *25* (4), 591−595.
(28) Zhou, H.; Yao, W.; Li, G.; Wang, J.; Lu, Y. Graphene/poly(3,4-ethylenedioxythiophene) hydrogel with excellent mechanical performance and high conductivity. *Carbon* **2013**, *59*, 495−502.
(29) Zhou, H.; Ni, T.; Qing, X.; Yue, X.; Li, G.; Lu, Y. One-step construction of graphene−polypyrrole hydrogels and their superior electrochemical performance. *RSC Adv.* **2014**, *4* (8), 4134−4139.
(30) Kovtyukhova, N. I.; Ollivier, P. J.; Martin, B. R.; Mallouk, T. E.; Chizhik, S. A.; Buzaneva, E. V.; Gorchinskiy, A. D. Layer-by-layer assembly of ultrathin composite films from micron-sized graphite oxide sheets and polycations. *Chem. Mater.* **1999**, *11*, 771−778.
(31) An, S. J.; Zhu, Y. W.; Lee, S. H.; Stoller, M. D.; Emilsson, T.; Park, S. J.; Velamakanni, A.; An, J.; Ruoff, R. S. Thin film fabrication and simultaneous anodic reduction of deposited graphene oxide platelets by electrophoretic deposition. *J. Phys. Chem. Lett.* **2010**, *1*, 1259−1263.
(32) Jiang, X.; Ma, Y. W.; Li, J. J.; Fan, Q. L.; Huang, W. Self-assembly of reduced graphene oxide into three-dimensional architecture by divalent ion linkage. *J. Phys. Chem. C* **2010**, *114*, 22462−22465.
(33) Bissessur, R.; Liu, P. K. Y.; Scully, S. F. Intercalation of polypyrrole into graphite oxide. *Synth. Met.* **2006**, *156* (16−17), 1023−1027.
(34) Dallas, P.; Niarchos, D.; Vrbanic, D.; Boukos, N.; Pejovnik, S.; Trapalis, C.; Petridis, D. Interfacial polymerization of pyrrole and in situ synthesis of polypyrrole/silver nanocomposites. *Polymer* **2007**, *48* (7), 2007−2013.
(35) Adhikari, B.; Biswas, A.; Banerjee, A. Graphene oxide-based supramolecular hydrogels for making nanohybrid systems with Au nanoparticles. *Langmuir* **2012**, *28* (2), 1460−1469.
(36) Zhang, K.; Zhang, L. L.; Zhao, X. S.; Wu, J. Graphene/polyaniline nanofiber composites as supercapacitor electrodes. *Chem. Mater.* **2010**, *22* (4), 1392−1401.
(37) He, Z.; Mansfeld, F. Exploring the use of electrochemical impedance spectroscopy (EIS) in microbial fuel cell studies. *Energy Environ. Sci.* **2009**, *2* (2), 215−219.
(38) Adhikari, B.; Biswas, A.; Banerjee, A. Graphene oxide-based hydrogels to make metal nanoparticle-containing reduced graphene oxide-based functional hybrid hydrogels. *ACS Appl. Mater. Interfaces* **2012**, *4* (10), 5472−5482.
(39) Pan, L. J.; Yu, G. H.; Zhai, D. Y.; Lee, R. H.; T, Z. W.; Liu, N.; Wang, H. L.; Tee, B.; Shi, Y.; Cui, Y.; Bao, Z. N. Hierarchical nanostructured conducting polymer hydrogel with high electrochemical activity. *Proc. Natl. Acad. Sci. U. S. A.* **2012**, *109* (24), 9287−9292.
(40) Frackowiak, E.; Beguin, F. Carbon materials for the electrochemical storage of energy in capacitors. *Carbon* **2001**, *39*, 937−950.
(41) Qiao, Y.; Bao, S. J.; Li, C. M.; Cui, X. Q.; Lu, Z. S.; Guo, J. Nanostructured polyaniline/titanium dioxide composite anode for microbial fuel cells. *ACS Nano* **2008**, *2* (1), 113−119.
(42) Ramasamy, R. P.; Veeraraghavan, B.; Haran, B.; Popov, B. N. Electrochemical characterization of a polypyrrole/$Co_{0.2}CrO_x$ composite as a cathode material for lithium ion batteries. *J. Power Sources* **2003**, *124* (1), 197−203.
(43) Luo, Y.; Jiang, J.; Zhou, W.; Yang, H.; Luo, J.; Qi, X.; Zhang, H.; Yu, D. Y. W.; Li, C. M.; Yu, T. Self-assembly of well-ordered whisker-like manganese oxide arrays on carbon fiber paper and its application as electrode material for supercapacitors. *J. Mater. Chem.* **2012**, *22* (17), 8634−8640.
(44) Liu, T.; Finn, L.; Yu, M.; Wang, H.; Zhai, T.; Lu, X.; Tong, Y.; Li, Y. Polyaniline and polypyrrole pseudocapacitor electrodes with excellent cycling stability. *Nano Lett.* **2014**, *14* (5), 2522−2527.
(45) Calvert, P. Hydrogels for soft machines. *Adv. Mater.* **2009**, *21* (7), 743−756.
(46) Wang, J.; Li, B.; Ni, T.; Dai, T.; Lu, Y. One-step synthesis of iodine doped polyaniline-reduced graphene oxide composite hydrogel with high capacitive properties. *Compos. Sci. Technol.* **2015**, *109*, 12−17.

DOI: 10.1021/sc500828t
ACS Sustainable Chem. Eng. 2015, 3, 862−870